REPORT DOCUMENTATION PAGE

Form Approved OMB NO. 0704-0188

1. REPORT DATE (DD-MM-YYYY)	2. REPORT TYPE	3. DATES COVERED (From - To)
15-02-2014	Final Report	1-Jun-2009 - 30-Nov-2013

4. TITLE AND SUBTITLE
Final Report: Probing Nanoparticle Reactivity at the Single-Molecule Level

5a. CONTRACT NUMBER
W911NF-09-1-0232

5b. GRANT NUMBER

5c. PROGRAM ELEMENT NUMBER
611102

6. AUTHORS
Peng Chen

5d. PROJECT NUMBER

5e. TASK NUMBER

5f. WORK UNIT NUMBER

7. PERFORMING ORGANIZATION NAMES AND ADDRESSES
Cornell University
Office of Sponsored Programs
373 Pine Tree Road
Ithaca, NY 14850 -2820

8. PERFORMING ORGANIZATION REPORT NUMBER

9. SPONSORING/MONITORING AGENCY NAME(S) AND ADDRESS (ES)
U.S. Army Research Office
P.O. Box 12211
Research Triangle Park, NC 27709-2211

10. SPONSOR/MONITOR'S ACRONYM(S)
ARO

11. SPONSOR/MONITOR'S REPORT NUMBER(S)
56355-CH.27

12. DISTRIBUTION AVAILIBILITY STATEMENT
Approved for Public Release; Distribution Unlimited

13. SUPPLEMENTARY NOTES
The views, opinions and/or findings contained in this report are those of the author(s) and should not contrued as an official Department of the Army position, policy or decision, unless so designated by other documentation.

14. ABSTRACT
This final report summarizes our achievements in developing and using single-molecule fluorescence microscopy techniques to interrogate and understand the surface reactivity of individual metal nanoparticles at an unprecedented level. The report covers: (1) Study of size-dependent catalytic activity and dynamics of Au nanoparticles at the single-molecule level (JACS 2010). (2) Quantitative super-resolution imaging of catalytic reactivity of single Au nanorods (Nat. Nanotechnol. 2012). (3) Site-specific activity mapping and discovery of radial activity gradients on single 2D nanocrystal catalysts (JACS 2013). (4) Development of a massively scalable

15. SUBJECT TERMS
single-molecule microscopy, single nanoparticle catalysis, super-resolution imaging, surface reactivity and dynamics

16. SECURITY CLASSIFICATION OF:			17. LIMITATION OF ABSTRACT	15. NUMBER OF PAGES	19a. NAME OF RESPONSIBLE PERSON
a. REPORT	b. ABSTRACT	c. THIS PAGE			Peng Chen
UU	UU	UU	UU		19b. TELEPHONE NUMBER 607-254-8533

Report Title

Final Report: Probing Nanoparticle Reactivity at the Single-Molecule Level

ABSTRACT

This final report summarizes our achievements in developing and using single-molecule fluorescence microscopy techniques to interrogate and understand the surface reactivity of individual metal nanoparticles at an unprecedented level. The report covers: (1) Study of size-dependent catalytic activity and dynamics of Au nanoparticles at the single-molecule level (JACS 2010). (2) Quantitative super-resolution imaging of catalytic reactivity of single Au nanorods (Nat. Nanotechnol. 2012). (3) Site-specific activity mapping and discovery of radial activity gradients on single 2D nanocrystal catalysts (JACS 2013). (4) Development of a massively scalable, parallel method for screening catalyst activity at the single-particle level and sub-diffraction spatial resolution (i.e., super-optical resolution) (ACS Catal. 2013). (5) Quantification of the catalytic activity and dynamics of single Pt nanoparticles in two different reactions (Nano Lett. 2012). (6) Discovery of long-range catalytic communication within single 1-D and 2-D nanocrystal catalysts. (7) Review of the theory and experiments as well as of the scientific insights from single-molecule nanoparticle catalysis studies (Nano Res. 2009, Phys. Chem. Chem. Phys. 2010, Chemical Society Reviews, 2010 & 2014). The report also describes our progress in the new direction of imaging catalytic reactivity at nanoscale metal?metal junctions.

Enter List of papers submitted or published that acknowledge ARO support from the start of the project to the date of this printing. List the papers, including journal references, in the following categories:

(a) Papers published in peer-reviewed journals (N/A for none)

Received		Paper
01/18/2014	26.00	Justin Sambur, Peng Chen. Approaches to Single-Nanoparticle Catalysis, Annual Review of Physical Chemistry, (01 2014): 0. doi:
01/30/2012	14.00	Kyu Sung Han, Guokun Liu, Xiaochun Zhou, Rita E. Medina, Peng Chen. How Does a Single Pt Nanocatalyst Behave in Two DifferentReactions? A Single-Molecule Study, Nano Letters, (01 2012): 0. doi:
02/01/2013	18.00	Nesha May Andoy, Xiaochun Zhou, Eric Choudhary, Hao Shen, Guokun Liu, Peng Chen. Single-Molecule Catalysis Mapping Quantifies Site-Specific Activity and Uncovers Radial Activity Gradient on Single 2D Nanocrystals, Journal of the American Chemical Society, (01 2013): 0. doi: 10.1021/ja309948y
02/19/2012	15.00	Nesha May Andoy, Xiaochun Zhou, Guokun Liu, Eric Choudhary, Kyu-Sung Han, Hao Shen, Peng Chen. Quantitative super-resolution imaging uncoversreactivity patterns on single nanocatalysts, Nature Nanotechnology, (02 2012): 0. doi:
06/03/2013	20.00	Xiaochun Zhou, Eric Choudhary, Nesha May Andoy, Ningmu Zou, Peng Chen. Scalable Parallel Screening of Catalyst Activity at the Single-Particle Level and Sub-diffraction Resolution, ACS Catalysis, (05 2013): 1448. doi:
06/16/2010	7.00	Hao Shen, Weilin Xu, Peng Chen. Single-molecule nanoscale electrocatalysis, Physical Chem Chem Physics, (07 2010): . doi:
09/19/2013	24.00	Peng Chen, Xiaochun Zhou, Nesha May Andoy, Kyu-Sung Han, Eric Choudhary, Ningmu Zou, Guanqun Chen, Hao Shen. Spatiotemporal catalytic dynamics within single nanocatalysts revealed by single-molecule microscopy, Chemical Society Reviews, (09 2013): 0. doi:
09/19/2013	25.00	Maicol Ochoa, Peng Chen, Roger Loring. Single Turnover Measurements of Nanoparticle Catalysis Analyzed with Dwell Time Correlation Functions and Constrained Mean DwellTimes, Journal of Physical Chemistry C, (09 2013): 0. doi:
11/07/2011	12.00	Maicol A. Ochoa, Xiaochun Zhou, Peng Chen, Roger F. Loring. Interpreting single turnover catalysis measurements with constrainedmean dwell times, J. Chem. Phys., (11 2011): 174509. doi:
12/10/2009	3.00	Weilin Xu, Hao Shen, Guokun Liu, Peng Chen. Single-Molecule Kinetics of Nanoparticle Catalysis, Nano Research, (10 2009): . doi:
12/10/2009	4.00	Xiaochun Zhou, Weilin Xu, Guokun Liu, Debashis Panda, Peng Chen. Size-Dependent Catalytic Activity and Dynamics of Gold Nanoparticles at the Single-Molecule Level, Journal of the American Chemical Society, (05 2009): . doi:
12/21/2010	8.00	P. Chen, X. Zhou, H. Shen, N. M. Andoy, E. Choudhary, K.-S. Han, G. Liu, W. Meng. Single-Molecule Fluorescence Imaging of Nanocatalytic Processes, Chemical Society Review, (05 2010): . doi:
TOTAL:	**12**	

Number of Papers published in peer-reviewed journals:

(b) Papers published in non-peer-reviewed journals (N/A for none)

Received Paper

TOTAL:

Number of Papers published in non peer-reviewed journals:

(c) Presentations

1) Symposium on “Chemistry at the Space-Time Limit”, ACS National Meeting, Indianapolis, IN; September, 2013; Spatial and Temporal Catalytic Dynamics on Single Nanoparticles
2) Symposium on "Catalytic Nanomaterials for Energy and Environment" MRS Fall Meeting, Boston, MA; December 1-6, 2013; Single-Molecule Super-resolution Imaging of Single-Nanoparticle Catalysis

Number of Presentations: 2.00

Non Peer-Reviewed Conference Proceeding publications (other than abstracts):

Received Paper

TOTAL:

Number of Non Peer-Reviewed Conference Proceeding publications (other than abstracts):

Peer-Reviewed Conference Proceeding publications (other than abstracts):

Received Paper

TOTAL:

Number of Peer-Reviewed Conference Proceeding publications (other than abstracts):

(d) Manuscripts

Received		Paper
01/12/2010	5.00	Hao Shen, Weilin Xu, Peng Chen. Single-Molecule Nanoscale Electrocatalysis, (12 2010)
02/07/2011	9.00	Peng Chen. Why Nanoparticle Catalysts Are Special: A Dynamic Adaptation Model, Nature Chemistry (02 2011)
05/15/2013	19.00	Xiaochun Zhou, Eric Choudhary, Nesha May Andoy, Ningmu Zou, Peng Chen. Scalable Parallel Screening of Catalyst Activity at the Single-Particle Level and Sub-diffraction Resolution, ACS Catalysis (04 2013)
05/29/2010	6.00	Peng Chen, Xiaochun Zhou, Hao Shen, Nesha May Andoy, Eric Choudhary, Kyu-Sung Han, Guokun Liu, Weilin Meng. Single-Molecule Fluorescence Imaging of Nanocatalysis, Chemical Society Review (05 2010)
08/06/2013	21.00	Peng Chen, Xiaochun Zhou, Nesha May Andoy, Kyu-Sung Han, Eric Choudhary, Ningmu Zou, Guanqun Chen, Hao Shen. Spatiotemporal Catalytic Dynamics within Single Nanocatalysts Revealed by Single-Molecule Microscopy, Chemical Society Review (06 2013)
08/06/2013	22.00	Maicol A. Ochoa, Peng Chen, Roger F. Loring. Single turnover measurements of nanoparticle catalysis analyzed with dwell time correlation functions and constrained mean dwell times, J Phys Chem C (07 2013)
08/22/2011	10.00	Xiaochun Zhou, Nesha May Andoy, Guokun Liu, Eric Choudhary, Kyu-Sung Han, Hao Shen, Peng Chen. Quantitative Super-resolution Imaging Uncovers Reactivity Patterns on Single Nanocatalysts, Nature Nanotechnology (08 2011)
08/23/2011	11.00	Xiaochun Zhou, Nesha May Andoy, Guokun Liu, Eric Choudhary, Kyu-Sung Han, Hao Shen, Peng Chen. Supporting info: Quantitative Super-resolution Imaging Uncovers Reactivity Patterns on Single Nanocatalysts, Nature Nanotechnology (08 2011)
08/24/2013	23.00	Justin Sambur, Peng Chen. Approaches to single nanoparticle catalysis, Annual Review of Physical Chemistry (08 2013)
11/11/2011	13.00	Guokun Liu, Xiaochun Zhou, Kyu Sung Han, Rita E. Medina, Peng Chen. How does a single Pt nanocatalyst behave in two different reactions? A single-molecule study, Nano Letters (11 2011)
11/29/2012	16.00	Nesha May Andoy, Xiaochun Zhou, Eric Choudhary, Hao Shen, Guokun Liu, Peng Chen. Single-Molecule Catalysis Mapping Quantifies Site-specific Activity and Uncovers Radial Activity Gradient on Single 2D Nanocrystals, J Am Chem Soc (10 2012)
12/01/2009	1.00	Weilin Xu, Hao Shen, Guokun Liu, Peng Chen. Single-Molecule Kinetics of Nanoparticle Catalysis, Nano Research (12 2009)
12/01/2009	2.00	Xiaochun Zhou, Weilin Xu, Guokun Liu, Debashis Panda, Peng Chen. Size Dependent Catalytic Activity and Dynamics of Gold Nanoparticles at the Single-Molecule Level, (12 2009)

12/20/2012 17.00 Xiaochun Zhou, Nesha May Andoy, Guokun Liu, Peng Chen. Long-range catalytic communications within single nanocatalysts,
Nature Chemistry (12 2012)

TOTAL: **14**

Number of Manuscripts:

Books

Received Paper

TOTAL:

Patents Submitted

Patents Awarded

Awards

2014 ACS PHYS Division Early-Career Award in Experimental Physical Chemistry
2014 Coblentz Award
2013 Honorable Lecturer, Applied Chemistry Lecture Series, Changchun Institute of Applied Chemistry, Chinese Academy of Sciences
2013 Peter J. W. Debye Professorship
2013 Lester S. Andrews Lecturer, Mississippi State University

Graduate Students

NAME	PERCENT_SUPPORTED	Discipline
Eric Choudhary	0.00	
Ningmu Zou	0.00	
Guanqun Chen	0.00	
FTE Equivalent:	**0.00**	
Total Number:	**3**	

Names of Post Doctorates

NAME	PERCENT_SUPPORTED
FTE Equivalent:	
Total Number:	

Names of Faculty Supported

NAME	PERCENT_SUPPORTED	National Academy Member
Peng Chen	0.00	
FTE Equivalent:	**0.00**	
Total Number:	**1**	

Names of Under Graduate students supported

NAME	PERCENT_SUPPORTED
FTE Equivalent:	
Total Number:	

Student Metrics

This section only applies to graduating undergraduates supported by this agreement in this reporting period

The number of undergraduates funded by this agreement who graduated during this period:	0.00
The number of undergraduates funded by this agreement who graduated during this period with a degree in science, mathematics, engineering, or technology fields:.....	0.00
The number of undergraduates funded by your agreement who graduated during this period and will continue to pursue a graduate or Ph.D. degree in science, mathematics, engineering, or technology fields:.....	0.00
Number of graduating undergraduates who achieved a 3.5 GPA to 4.0 (4.0 max scale):.....	0.00
Number of graduating undergraduates funded by a DoD funded Center of Excellence grant for Education, Research and Engineering:.....	0.00
The number of undergraduates funded by your agreement who graduated during this period and intend to work for the Department of Defense	0.00
The number of undergraduates funded by your agreement who graduated during this period and will receive scholarships or fellowships for further studies in science, mathematics, engineering or technology fields:	0.00

Names of Personnel receiving masters degrees

NAME
Total Number:

Names of personnel receiving PHDs

NAME
Total Number:

Names of other research staff

NAME	PERCENT_SUPPORTED
FTE Equivalent:	
Total Number:	

Sub Contractors (DD882)

Inventions (DD882)

Scientific Progress

See attachment

Technology Transfer

Proposal #: 56355-CH
Agreement #: W911NF0910232
Title: Probing Nanoparticle Reactivity at the Single-Molecule Level
PI: Peng Chen, Department of Chemistry and Chemical Biology, Cornell University

Final Report: Scientific Progress and Accomplishments (06/01/2009 – 11/30/ 2013, including no cost extension from 5/31/13 to 11/30/13)

Table of content

Summary of report

The overall objective of our funded research is to develop and use single-molecule fluorescence microscopy techniques to interrogate and understand the surface reactivity of individual metal nanoparticles at an unprecedented level. During the funding period, we have made the following accomplishments:

1) Study of size-dependent catalytic activity and dynamics of Au nanoparticles at the single-molecule level (*JACS* **2010**)[1]
2) Quantitative super-resolution imaging of catalytic reactivity of single Au nanorods (*Nat. Nanotechnol.* **2012**)[2].
3) Site-specific activity mapping and discovery of radial activity gradients on single 2D nanocrystal catalysts (*JACS* **2013**)[3].
4) Development of a massively scalable, parallel method for screening catalyst activity at the single-particle level and sub-diffraction spatial resolution (i.e., super-optical resolution) (*ACS Catal.* **2013**)[4].
5) Quantification of the catalytic activity and dynamics of single Pt nanoparticles in two different reactions (*Nano Lett.* **2012**)[5].
6) Discovery of long-range catalytic communication within single 1-D and 2-D nanocrystal catalysts (manuscript in revision for *Nature Chemistry*)[6].
7) Review of the theory and experiments as well as of the scientific insights from single-molecule nanoparticle catalysis studies (*Nano Res.* **2009**, *Phys. Chem. Chem. Phys.* **2010**, *Chemical Society Reviews*, **2010 & 2014**)[7-10].

We have further made progress in the following new directions:

8) Imaging catalytic reactivity at nanoscale metal–metal junctions.

In the following I summarize our accomplishments (#1-6) above and progress in (#8) above.

I. Size-dependent catalytic activity and dynamics of single Au nanoparticles (*JACS* 2010)[1]

We have studied how the catalytic activity, selectivity, and dynamic surface restructuring of pseudospherical Au nanoparticles depend on the nanoparticle size, i.e., diameter. We have studied three different sizes in detail: 6.0 ± 1.7 nm, 9.1 ± 1.5 nm, and 13.7 ± 2.4 nm. The major insights we learned include:

1) The catalytic activity of these pseudospherical particles show strong size dependence, as manifested by the size dependence of their associated kinetic parameters in the reaction mechanism (**Fig 1**), including K_1, the substrate adsorption equilibrium constant, γ_{eff}/A, the catalytic rate constant per surface area (A), k_2, the product dissociation rate constant in the substrate-assisted pathway, and k_3, the rate constant for direct product dissociation. These size-dependences can all be quantitatively analyzed using a classical thermodynamic model, which approximates a metal nanoparticle as a continuous phase and attributes its size effect to changes in its chemical potential from surface tension.

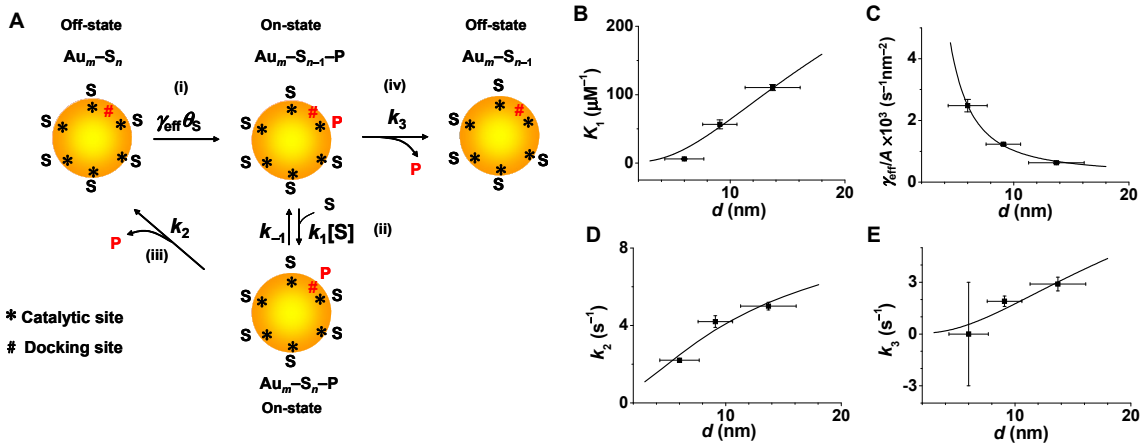

Fig 1. Kinetic mechanism and size-dependent catalytic activity. (A) Schematic of the kinetic mechanism. Au$_m$: Au nanoparticle; S: resazurin; P: resorufin. Au$_m$-S$_n$ represents a Au nanoparticle having n adsorbed substrate molecules at adsorption equilibrium. The fluorescence state (on or off) of the nanoparticle is indicated at each reaction stage. $\gamma_{eff} = kn_T$ and represents the combined reactivity of all surface catalytic sites of a nanoparticle. k is a rate constant representing the reactivity per catalytic site for the catalytic conversion. n_T is the total number of surface catalytic sites on one Au nanoparticle. θ_S is the fraction of catalytic sites that are occupied by substrates and equals $K_1[S]/(1+K_1[S])$, where K_1 is the substrate adsorption equilibrium constant. (B-E) Thermodynamic analyses of the size dependences of kinetic parameters. Solid lines are fits from a classical thermodynamic model.

2) These nanoparticles show size-dependent selectivity between the two parallel product dissociation pathways in **Fig 1A**. Their different selectivity gives rise to three types of catalytic behaviors, denoted as type I, II, and III in **Fig 2** — The subpopulations among the three types of catalytic behaviors shift when the particle size changes.
3) These nanoparticles all show surface-restructuring-coupled temporal catalytic dynamics (e.g., **Fig 3A**), but the timescale of the underlying dynamic surface restructuring shows strong dependence on the particle size and the catalytic turnover rates (**Fig 3B**). We were able to extract approximate energetics for spontaneous surface restructuring that is fundamentally important for heterogeneous catalysis.

d (nm)	Type I ($k_2 > k_3$)	Type II ($k_2 < k_3$)	Type III ($k_2 \approx k_3$)
6.0	66%	19%	15%
9.1	66%	11%	23%
13.7	43%	6%	51%

Fig 2. Size-dependent relative subpopulations of Type I, II, and III kinetic behaviors.

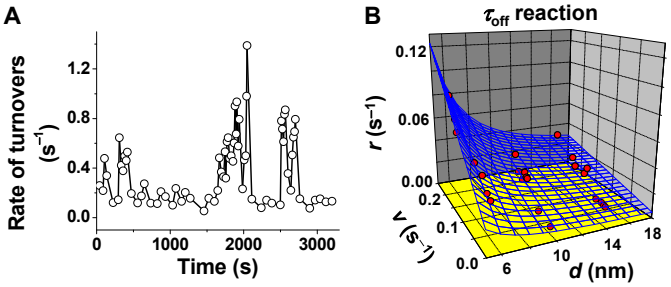

Fig 3. Surface-restructuring-coupled temporal catalytic dynamics. (A) Trajectory of rate of turnovers for a single 6-nm Au nanoparticle at a saturating substrate concentration. (B) Surface restructuring rate (r) dependence on the rate of turnovers (v) and the nanoparticle diameter (d). Dots are experimental data. The meshed surface is a fit with a thermodynamic model.

The *significances* of this achievement are that (1) it provides quantitative understanding how size can change and tune the nanoparticle's catalytic activity and selectivity, and (2) how the size affects the energetics and timescales of surface restricting dynamics and its coupling to temporal catalytic behaviors, both of which are fundamentally important to surface catalysis at the nanoscale.

II. Quantitative super-resolution imaging of catalytic reactivity of single Au nanorods (*Nat. Nanotechnol.* 2012)[2]

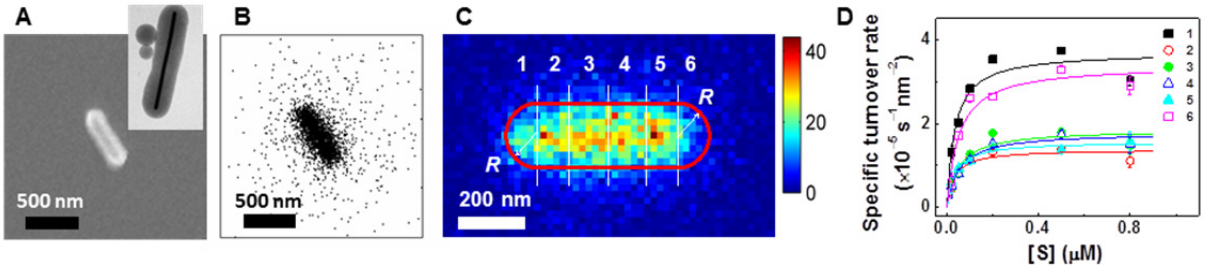

Fig 4. Quantitative super-resolution imaging of single Au@mSiO$_2$ nanorod catalysis. (A) SEM of a Au@mSiO$_2$ nanorod. Inset: TEM image a Au@mSiO$_2$ nanorod. (B) Positions of product (**P**) molecules detected on the nanorod in (A). Each dot is one **P** molecule. The reactions were performed with 0.02–0.8 μM amplex red, 60 mM H_2O_2 in 7 mM pH 7.3 phosphate buffer. (C) 2-dimensional histogram of (B) in 20×20 nm^2 bins. The orientation of the image has been rotated so that the nanorod lies horizontally. The red line is the outer structural contour from its SEM image in (A), which encircles the silica shell. Vertical lines dissect the nanorod into 6 segments; For clarity, (B) only includes the first ~2800 of ~8700 **P** molecules presented in (C). (D) [S] dependence of specific turnover rates of the segments from (C). All error bars are s.e.m.

Using mesoporous-encapsulated Au nanorods (i.e., Au@mSiO$_2$ nanorods) as model pseudo-1-D nanocatalysts (**Fig 4A**), we have used single-molecule, super-resolution fluorescence microscopy to spatially resolve catalysis on single nanocatalysts to differentiate reactivity at different locations on a single nanocrystal catalyst. In this approach, we individually image and localize the positions of each reaction product (**P**) catalytically generated on a single nanorod at nanometer precision. By localizing the position of every **P** molecule, we mapped all catalytic reactions on a single Au@mSiO$_2$ nanorod (**Fig 4B**). Both this map and the 2-dimensional histogram (**Fig 4C**) of the **P** positions clearly resolve the rod shape. The spatial resolution here is ~40-nm,[2] comparable to related super-resolution optical microscopy techniques[11-13]. The wide-field imaging format here further offers studying hundreds of nanorods in parallel, giving a high data throughput. With the SEM image on the same nanorod (**Fig 4A**), We were able to map its SEM structural contour onto the 2-dimensional histogram of its **P** positions and dissect the nanorod into ~90-nm segments (**Fig 4C**). For each segment, we determined its specific turnover rate, *v*, by counting the number of **P** molecules per unit time and per Au surface area, and from its dependence on the reactant concentration (**Fig 4D**), we determined *k*, the specific catalytic rate constant, and *K*, the adsorption equilibrium constant of each segment, which directly quantify the catalytic property of a single nanorod at sub-particle resolution. The major insights we learned include:

1) In general (~85% of the nanorods), the nanorod ends have higher catalytic reactivity (i.e., larger rate constants) than their sides (**Fig 5A**).
2) The relative reactivity between the ends and the sides of a Au nanorod is *not* in-

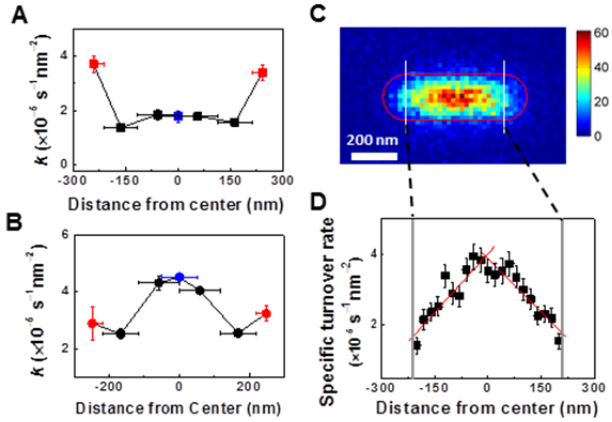

Fig 5. Spatial reactivity patterns on single Au@mSiO$_2$ nanorods. (A) An exemplary nanorod whose ends have higher catalytic reactivity (i.e., larger specific catalytic rate constant *k* than its side facets. End-segments highlighted in red; center-segment in blue. (B) Same as in (A), but for another nanorod. (C) 2-dimensional histogram of ~9530 **P** positions from the nanorod in B in 20 × 20 nm^2 bins. The vertical lines separate out the end-segments. (D) Dependence of the specific turnover rate, *v*, on the location along the length of the nanorod in (C). The nanorod is sliced into ~20-nm segments.

variant and some nanorods (~15% of them) have their sides more reactive than their ends (**Fig 5B**). This variant behavior is completely hidden in results averaged over many nanorods.

3) More surprisingly, within the side facets of any single nanorod, the reactivity is not constant, but rather shows a reactivity gradient from the center toward the two ends (**Fig 5C, D**). We attributed this reactivity gradient to an underlying defect density gradient on the side facets, which resulted from the non-uniform one-dimensional growth rate during nanorod synthesis[14].

The *significances* of these findings are that (1) they uncovered the complexity of spatial reactivity patterns at the nanoscale, and (2) they demonstrated that knowing the surface-facets of shaped-controlled nanocrystal catalysts is insufficient for correlating with their reactivity, as the reactivity can differ significantly even within the same facets. Surface defects need to be examined as well, and they are abundant on nanocatalysts and are strongly affected by the growth rate and the synthesis procedure of the nanocatalysts, both of which can play dominant roles in determining their surface reactivity. Certainly, the importance of surface defects in catalysis is well known from surface science[15], but their presence is challenging to determine on nanocrystal surfaces, even with advanced electron microscopy[16]. By spatially resolving catalytic reactions at the nanometer resolution on single nanocatalysts, we have demonstrated the power of this approach in unraveling the complexity of reactivity at the nanoscale.

III. Site-specific activity mapping and discovery of radial activity gradients on single 2D nanocrystal catalysts (*JACS* 2013)[3]

In parallel to our previous work on Au@mSiO_2 nanorods where we discovered complex reactivity patterns on pseudo-1D nanocrystals[2], we also studied the pseudo-2D nanocrystal catalysts, triangular and hexagonal Au@mSiO_2 nanoplates (**Fig 6A**), in order to probe if complex spatial activity patterns exist beyond 1D nanocrystals. These Au nanoplate cores are single crystals with edge length of ~10 – 1000 nm and thickness of ~14 nm. Their large top and bottom flat surfaces are (111) facets, and the edges are (111) or (100) facets[17,18]. Moreover, to diversify the types of catalytic transformations, we studied the reductive N-deoxygenation of resazurin to resorufin by NH_2OH, as compared to the oxidative N-deacetylation reaction of amplex red to resorufin by H_2O_2.

Using the single-molecule super-resolution imaging approach, we localized the positions of individual catalytic products on single Au@mSiO_2 nanoplates, and mapped them onto their SEM images (**Fig 6B** and **C**). This mapping immediately allowed us to dissect individual Au@mSiO_2 nanoplates and the associated product locations into three types of regions: corners, edges, and flat top facets (**Fig 6C**), and within the top facets, further into different radial segments (**Fig 6D**). The scientific insights we learned included:

1) Within any single nanoplate, the specific activity follows the trend of corners > edges > flat facets (**Fig 6E**). And the trend persists when averaged over >50 Au@mSiO_2 nanoplates of different sizes. This trend could be rationalized by the percentage of available low-coordination surface sites that decreases from corners to edges to facets.
2) The nanoplates, either each analyzed as a whole unit or each spatially dissected into different regions, show strong size-dependent specific catalytic activity, with larger ones having lower specific activity. This side dependence can be accounted for by their size-dependent chemical potentials, similar to the size-dependent activity of pseudo-spherical Au nanoparticles we studied previously[1].
3) Surprisingly, but consistent with our findings on Au nanorods, the specific activities among the radial segments within the same flat facet of a single nanoplate are *not* uniform, and instead show a clear radial gradient, highest at the center of the facet and decays approximately linearly toward the periphery (**Fig 6D, F**). We attributed this radial activity gradient of Au nanoplates to an underlying radial gradi-

ent of surface defect density that came from the decaying growth rate when the nanoplate grew in 2D from a seed during their synthesis.

The *significances* of these findings are that (1) they offer most direct site-specific activity information on single nanocrystal catalysts, and (2) they show that activity gradients within the same crystal facets exist beyond 1D nanocrystals even in a different catalytic transformation. The latter further corroborates that for understanding the catalytic activity of shape-controlled nanocrystals, knowing their facet assignments is insufficient. High-resolution activity studies are needed, where single-molecule approach provides an advantage, and high-resolution structural studies are also needed to probe the surface structure of these nanocrystals so that knowledge from surface science or theory can be suitably applied.

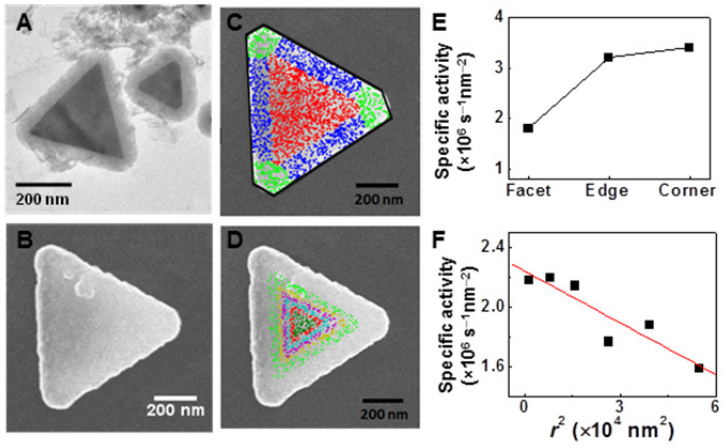

Fig 6. Spatial reactivity patterns on single Au@mSiO$_2$ nanoplates. (A) TEM image of two triangular Au@mSiO$_2$ nanoplates. (B) SEM image of a triangular Au@mSiO$_2$ nanoplate. (C) Locations of 2325 product molecules overlaid on top of the SEM image of the Au@mSiO$_2$ nanoplate in B. Each dot is the location of one product molecule. The locations are color-coded according to their respective regions on the nanoplate: flat facet (red), edges (blue) and corners (green). The solid black line outlines the outer contour of the mSiO$_2$ shell. The dashed black line outlines the perimeter of the Au nanoplate core. (D) Locations of 1055 product molecules overlaid on top of the SEM image of a Au@mSiO$_2$ nanoplate in B. The facets (i.e., top and bottom) are divided into radial segments from the center toward the periphery; the product locations in different segments are colored differently. The product molecules residing in the corner and edge regions are excluded here. (E) Specific activities of the different regions of the nanoplate from C. (F) Dependence of specific activities of radial segments on r^2 for the nanoplate in D. r is the distance between the center of the nanoplate and the midpoint of the segment along the center-to-corner vector. Solid line is a linear fit.

IV. Development of a massively scalable, parallel method for screening catalyst activity at the single-particle level and sub-diffraction spatial resolution (i.e., super optical resolution) (*ACS Catal.* 2013)[4]

For catalyst discovery and optimization, once the catalysts are made or modified, one always needs to screen their activity, where high data throughput and quantitative activity information are desired. Along this line, we have further developed our single-molecule fluorescence microscopy approach into a massively scalable, parallel method for screening catalyst activity, using the two fluorogenic probe reactions (one an N-deacetylation reaction and the other an N-deoxygenation reaction). This method offers the following capabilities:

1) Its wide field imaging format allows imaging the catalysis on a large number of catalyst particles in parallel, giving high data throughput. For example, **Fig 7A** shows the results on ~1000 particles. With motorized microscopes and larger camera formats, one can image even larger areas of samples to screen many more particles.
2) It offers sub-diffraction spatial resolution, i.e., super optical resolution, similarly as described in Section I above, where individual particles can be resolved (**Fig 7A, B**).

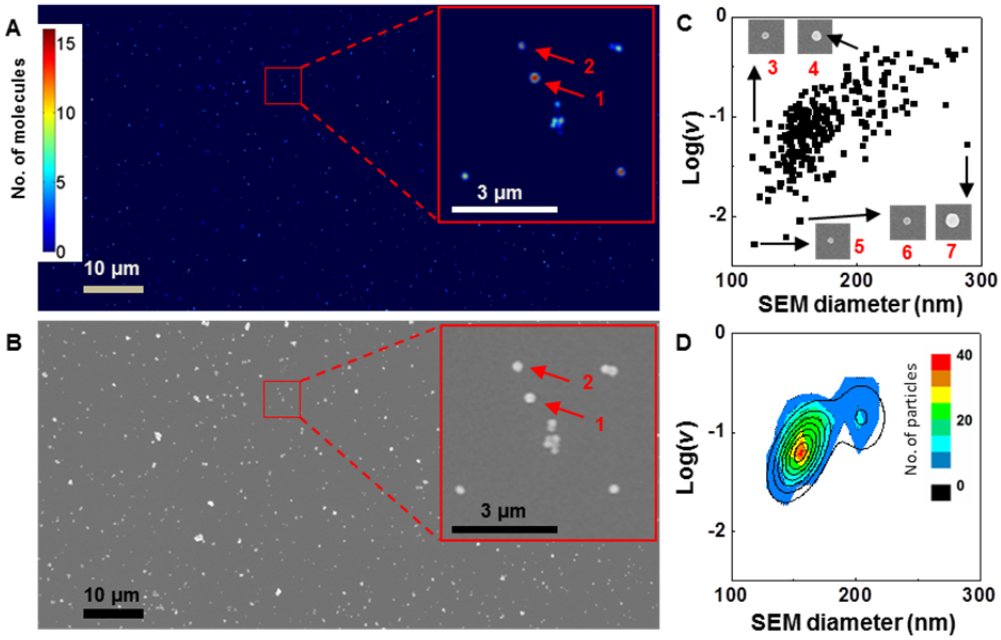

Fig 7. Parallel activity screening of a mixture of pseudo-spherical 21@42 nm and 102@32 nm (core-diameter@shell-thickness) Au@mSiO$_2$ particles in catalyzing the reductive N-deoxygenation of resazurin to resorufin. (A) Sub-diffraction catalysis image of ~1000 particles. This image is a 2-D histogram of product locations that were mapped at the single-molecule level. (B) SEM image of the same set of particles as in A. (C) Scatter plot of individual catalyst particles against their respective SEM diameter and rate of turnovers (v, in s^{-1} particle^{-1} in log scale). Each point represents one particle. Insets are SEM images of selected particles indicated by arrows. (D) Contour plot of the 2-D histogram of C, where the two subpopulations are clearly resolved.

3) It offers quantitative activity information of every catalyst particle, which can be directly correlated to its structural properties, such as its size from SEM (**Fig 7C**).
4) It can resolve subpopulations readily, such as in a binary mixture of catalyst particles (**Fig 7D**).
5) Although it is based on fluorogenic probe reactions, we have shown that the activities of catalyst particles in the two fluorogenic catalytic reactions are directly correlated with standard model catalytic reactions such as 4-nitrophenol reduction and hydroquinone oxidation (**Fig 8A, B**), so their activities in the fluorogenic probe reactions can be extrapolated and generalized to other non-fluorogenic reactions.

The *significance* of this achievement is that it offers a massively scalable, parallel method for screening catalyst activity quantitatively at the single-particle level, which further provides an opportunity to couple high-resolution TEM to examine the structure of the high activity particles identified. By correlating the activity in the probe reactions with other reactions of industrial relevance, this method can provide an effective approach for catalyst discovery and development.

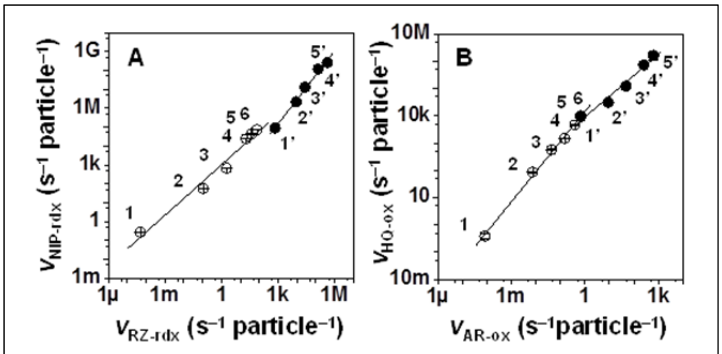

Fig 8. Activity correlation for the same set of catalyst particles between two different reactions. (A) Between the reductive N-deoxygenation reaction of resazurin (i.e., RZ-rdx) and the reduction of 4-nitrophenol (i.e., NIP-rdx). (B) Between the oxidative N-deacetylation reaction of amplex red (i.e., AR-ox) and the oxidation of hydroquinone (i.e., HQ-ox). The activities were measured at the ensemble level and quantified by the rate of turnovers (v). Two series of catalyst particles were tested: one (●), bare pseudo-spherical Au particles of 5, 10, 20 100, and 250 nm in diameter, denoted as 1′, 2′, 3′, 4′, and 5′; and the other (○), pseudo-spherical Au@mSiO$_2$ particles of 6@38, 22@80, 42@65, 42@70, 60@83, 102@59 nm in size (core-diameter@shell-thickness), denoted as 1, 2, 3, 4, 5, and 6, in the plots.

V. Qunatification of the Catalytic activity and dynamics of single Pt nanoparticles in two different reactions (*Nano Lett.* 2012)[5]

Most metal nanoparticles can catalyze a multitude of chemical transformations, for example Pt nanoparticles can catalyze both oxidative and reductive reactions[15]. For a particular type of nanoparticles, its activities in catalyzing these different reactions can be correlated to each other or have little correlation, as different reactions may occur at different surface sites on the same nanoparticle. Considering the inherent heterogeneity of nanoparticle catalysts, a fundamental question then arises: *how would the catalytic behavior of a single nanoparticle be correlated between different reactions*? An answer to this question will contribute to understanding the structure-activity correlation of nanoparticle catalysts across a variety of chemical transformations. Along this line, we have studied the catalysis of individual Pt nanoparticles in two reactions, one an oxidative N-deacetylation reaction and the other a reductive N-deoxygenation reaction (**Fig 9B**). This achievement capitalizes on our earlier work of developing a *single-molecule fluorescence microscopy approach* to study Au nanoparticle catalysis at the single-particle and single-turnover resolution (*Nature Mater.* **2008**[19]). In this approach, total internal reflection fluorescence microscopy and a fluorogenic catalytic reaction are used, and the fluorescence signal of a reaction product is imaged at the single-molecule level in real time (**Fig 9A**).

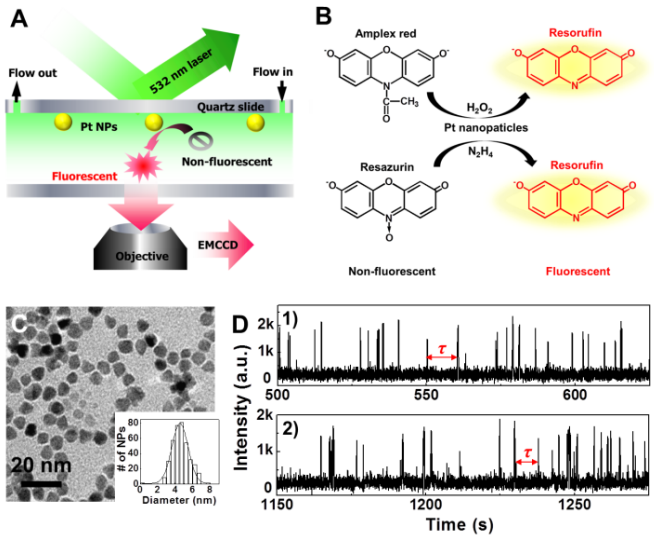

Fig 9. (A) Experimental scheme of single-molecule fluorescence measurements of catalysis by individual nanoparticles using total-internal-reflection fluorescence microscopy of fluorogenic reactions. (B) Pt-nanoparticle-catalyzed oxidative *N*-deacetylation of amplex red by H_2O_2 and reductive *N*-deoxygenation of resazurin by N_2H_4. Both reactions lead to formation of the fluorescent resorufin. (C) TEM image of Pt nanoparticles. Inset: diameter distribution of Pt nanoparticles; NPs = nanoparticles; Gaussian fit gives an average diameter of 4.6 ± 0.9 nm. (D) Exemplary fluorescence intensity versus time trajectories of single Pt nanoparticles under catalysis for 1) the oxidative *N*-deacetylation reaction at 5 μM amplex red and 200 mM H_2O_2 and 2) the reductive *N*-deoxygenation reaction at 0.2 μM resazurin and 1 mM N_2H_4. Time resolution: 20 ms. τ is the microscopic reaction time between sequential reaction events, which are manifested by the fluorescence intensity bursts.

We chose Pt nanoparticles as the catalyst of interest, with the additional purpose of extending our single-molecule study from Au particles to more industry relevant catalysts. These are *citrate-stabilized* colloidal Pt nanoparticles of 4.6 ± 0.9 nm in diameter and have faceted shapes of cube, tetrahedron, or cube-octahedron (**Fig 9C**). Using the approach as in **Fig 9A**, we monitored single Pt nanoparticles in catalyzing the two fluorogenic reactions sequentially. **Fig 9D** shows the time trajectories of fluorescence intensities from two Pt nanoparticles, each undertaking one of the two catalytic reactions. The fluorescence bursts report the individual catalytic turnovers. Our specific achievements in this study included:

1) Discovery that Pt nanoparticles show distinct catalytic kinetics in these two reactions: the reactants in the N-deacetylation reaction follow noncompetitive adsorption while those in the N-deoxygenation reaction follow competitive adsorption within the model of Langmuir-Hinshelwood kinetics.
2) Quantification of the large activity heterogeneity among individual Pt nanoparticles.

3) Discovery and quantification that in both reactions, individual Pt nanoparticles show temporal activity fluctuations, attributable to dominantly spontaneous dynamic surface restructuring, whose timescale is about tens of seconds, slower than that of Au nanoparticles of similar diameter.
4) Discovery that when catalyzing both reactions sequentially, and depending on the reaction sequence, single Pt nanoparticles may or may not show activity correlations between these two reactions, reflecting their structure sensitivity in the N-deoxygenation reaction and structure insensitivity in the N-deacetylation reaction.

The *significances* of this study include: (1) It demonstrates that the single-molecule approach is applicable to other metals of more industrial relevance, such as Pt, besides Au we studied previously[1,19-21]. (2) It further demonstrates that nanoparticle catalysts are dynamic entities, whose temporal activity behaviors carry important information on their structural properties and the coupling between dynamic structure and temporal activity. (3) Single-particle analysis in different reactions can inform on the structural sensitivity or insensitivity of the catalyst, complementary to ensemble methods that often rely on the examination of the size-dependence of the catalytic activity[22].

VI. Discovery of long-range catalytic communication within single 1-D and 2-D nanocatalysts (manuscript in revision for *Nature Chemistry*)

For catalysis, nature's most efficient nanoscale catalysts are enzymes. One of the distinguishing features of enzymes, or proteins broadly, is allosteric effects, in which the binding of a substrate or ligand at one site affects the binding or catalysis at another site without direct interaction between the two lig-

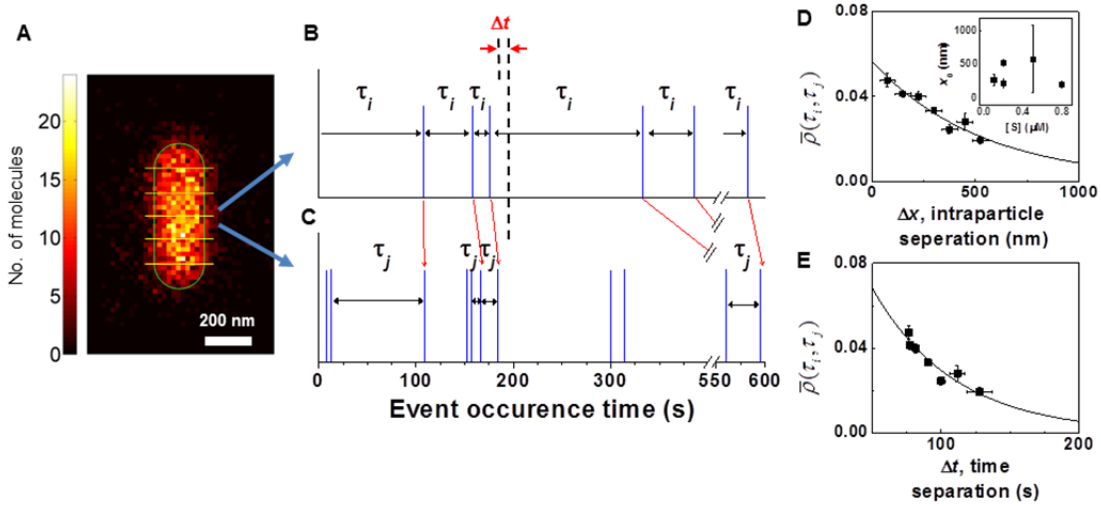

Fig 10. Long-range catalytic communication within single Au@mSiO$_2$ nanorods. (A) 2-D histogram of product locations on a single nanorod. The green line is the outer structural contour from its SEM image. The horizontal yellow lines dissect the nanorod into ~90 nm long segments. (B, C) Two catalytic event sequences for the two center segments (*i* and *j* segments) of the nanorod in A. In each sequence, the individual product detection events (vertical lines) were plotted against the times when they were detected. The microscopic reaction time for each event is the time separation from the previous one in the same sequence. Pairs of reactions that neighbor in time but occur at two different segments are linked by red arrows. The time separation (Δt) is illustrated for a pair of temporally neighboring catalytic events, each occurring at one of the two segments. (D) Dependence of the Pearson's correlation coefficient, $\bar{\rho}(\tau_i, \tau_j)$, on the intra-nanorod distance separation, Δx, between the segments. Δx is defined as the geometric center-to-center distance between two segments on the same nanorod. The first point in the plot is for two neighboring segments in a same nanorod. Solid line is a fit with $\rho_x e^{-\Delta x/x_0}$ with $\rho_x = 0.057 \pm 0.003$ and $x_0 = 530 \pm 50$ nm. x_0 represents a catalytic communication distance. Inset, the communication distance, x_0, obtained at different concentrations of the reactant amplex red ([S]) while [H_2O_2] is kept at excess at 60 mM. (E) Dependence of $\bar{\rho}(\tau_i, \tau_j)$ on the average time separation, Δt, of the temporally neighboring reactions at two different segments on the same nanorod. Solid line is a fit with $\rho_t e^{-\Delta t/t_0}$ with $\rho_t = 0.16 \pm 0.04$ and $t_0 = 59 \pm 10$ s. t_0 represents a temporal memory of the catalytic communication. Data here are averaged over >1100 segments from >220 nanorods. Y error bars are s.e.m. X error bars in D are half of the average segment length and in E are s.d.

ands or substrates[23,24]. Can reactions at different surface sites on the same nanoparticle communicate with each other, similarly as in allosteric enzymes? We have found that they do, by analyzing the correlation between individual, temporally neighboring reactions that occur at different locations on a single Au nanocatalyst.

To reach our discovery, we first used single-molecule super-resolution fluorescence microscopy to resolve individual reactions spatially on single nanocatalysts in real time, as described in Section I above. **Fig 10A** shows the 2-D histogram of reaction product locations on a single Au@mSiO$_2$ nanorod in catalyzing the oxidative N-deacetylation reaction of amplex red to resorufin, as we reported previously[2]. This mapping allowed us to dissect the nanorod, as well as its catalytic product positions, into segments along its long axis. For each segment, the catalytic product molecules can be arranged in a sequence of catalytic events according to when each product molecule was detected, i.e., when the catalytic reaction occurred. **Fig 10B** and **C** show such event sequences for two adjacent segments of the nanorod in **Fig 10A**. For each sequence, the time separation (τ) between a catalytic event and the previous event is the microscopic reaction time for generating this catalytic product at the respective segment; its individual values are probabilistic, but $\langle\tau\rangle^{-1}$, where $\langle\ \rangle$ denotes averaging, corresponds to the rate of catalytic turnovers for that nanorod segment. We then analyzed the correlation of the microscopic reaction time τ for reactions that neighbor in time but occur at different segments on the same nanorod; the correlation is quantified by a Pearson's correlation coefficient $\bar{\rho}(\tau_i, \tau_j)$ where the microscopic reaction time τ_i on segment *i* is paired with τ_j of the immediate subsequent catalytic event that occurs at segment *j* and vice versa (**Fig 10B, C**). $\bar{\rho}(\tau_i, \tau_j)$ is a quantitative measure of how the microscopic reaction kinetics, reflected by τ, of *temporally* neighboring reactions at two different segments are linearly correlated with each other.

We analyzed >200 nanorods using the above analysis. We further performed the analysis on >50 Au@mSiO$_2$ nanoplates (**Fig 11A-C**) in catalyzing the reductive N-deoxygenation reaction, where we divided each nanoplate into square segments and extracted the catalysis event sequences of each segment as in **Fig 10B** and **C**. By pooling all data together, we made the following major findings:

1) For nanorods, between two adjacent segments within a single nanorod, $\bar{\rho}(\tau_i, \tau_j)$ is 0.047 ± 0.003, which is a positive, although small, value (error is s.e.m., **Fig 10D**). This positive value indicates that reactions occurring at adjacent segments do communicate with each other: a reaction with a short τ, i.e., a fast reaction, at one segment tends to be followed by another fast reaction at the other segment, giving rise to a *phenomenological positive cooperativity*. Nonetheless, this communication is weak, as reflected by the small magnitude of $\bar{\rho}(\tau_i, \tau_j)$.
2) For nanorods, with increasing intraparticle separation (Δx) between the segments, $\bar{\rho}(\tau_i, \tau_j)$ gradually decreases, following an approximate exponential decay (**Fig 10D**). Strikingly, the exponential decay distance x_0 is 530 ± 50 nm, which indicates that a catalytic reaction on a Au@mSiO$_2$ nanorod can communicate with another reaction at ~500 nm away! This catalytic communication distance is about two orders of magnitude longer than that in allosteric enzymes, whose allosteric sites are typically just a few angstroms to a few nanometers apart. Moreover, x_0 is essentially independent of the reactant concentration over a range in which the turnover rate changes significantly (**Fig 10D** inset). Therefore, the catalytic communication distance x_0 is likely not determined by the catalytic condition, but rather characteristic to these Au@mSiO$_2$ nanorods.
3) For nanorods, $\bar{\rho}(\tau_i, \tau_j)$further decreases gradually with the averaging time separation (Δt) between the pair of reactions, and the decrease follows approximately an exponential decay function, with a decay time constant t_0 of 59 ± 10 s (**Fig 10E**). Physically, t_0 represents a temporal memory, i.e., the time that a subsequent catalytic reaction can "remember" an earlier reaction that occurred on the same nanocatalyst.
4) For nanoplates, $\bar{\rho}(\tau_i, \tau_j)$ is again positive, 0.039 ± 0.005 (error is s.e.m. **Fig 11D**), when the intraparticle distance separation between the segments is about 150 nm, similar to that between neighboring segments of nanorods. Therefore, reactions occurring at different locations on a single nanoplate

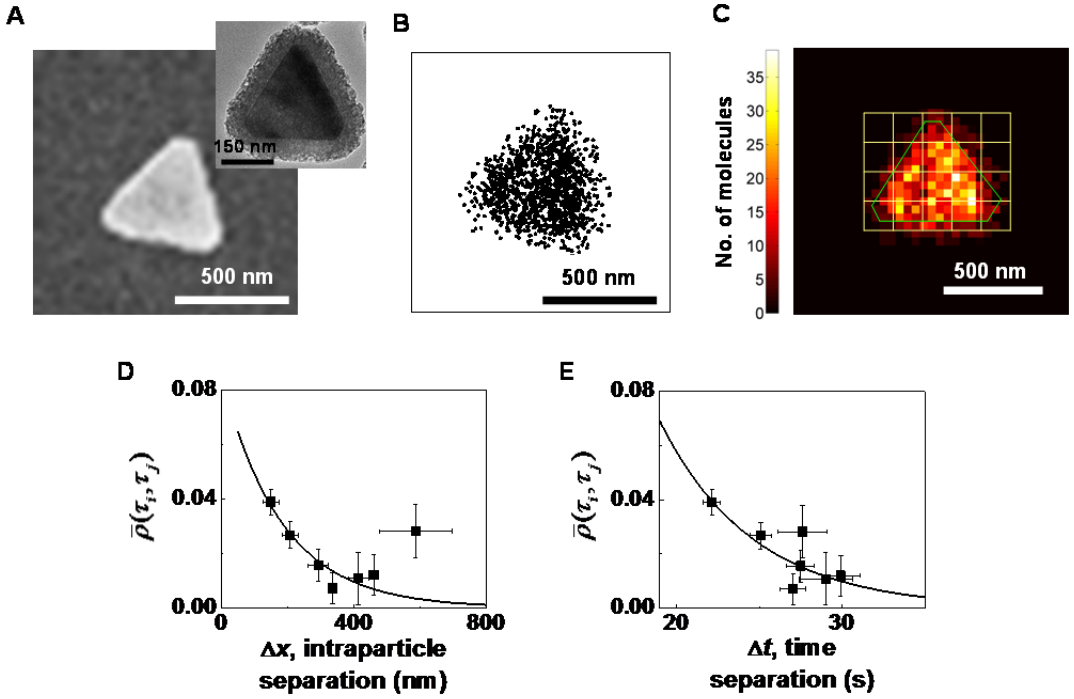

Fig 11. Long-range catalytic communication within single Au@mSiO$_2$ nanoplates. a, SEM of a triangular Au@mSiO$_2$ nanoplate. Inset, TEM of a representative Au@mSiO$_2$ nanoplate. b, Positions of ~2350 P molecules from the reductive N-deoxygenation reaction of resazurin detected on the nanoplate in a. Each dot is one P molecule. c, 2-D histogram of b in 40 × 40 nm^2 bins. The orientation of the plot has been rotated so that one edge of the nanoplate aligns horizontally. The green line is the outer structural contour from its SEM image in a. The yellow lines dissect the nanoplate into ~150 × 150 nm^2 square segments. d, e, Dependence of the Pearson's correlation coefficient, $\bar{\rho}(\tau_i, \tau_j)$, on the intra-nanoplate distance separation, Δx, between the segments and the time separation, Δt, of the neighboring reactions at two different segments on the same nanoplate. Solid lines are fits as in Fig. 3a and b, with ρ_x = 0.09 ± 0.03 and x_0 = 183 ± 50 nm, and ρ_t = 2.0 ± 2.0 and t_0 = 5.7 ± 1.4 s. Data averaged over ~520 segments from ~50 nanoplates. Y error bars are s.e.m. X error bars are s.d.

also communicate with each other. $\bar{\rho}(\tau_i, \tau_j)$ also shows decay behaviors with increasing intraparticle distance separation Δx and average time separation Δt (**Fig 11D, E**). The corresponding distance constant x_0 is 183 ± 50 nm, giving the catalytic communication distance, and the time constant t_0 is of 5.7 ± 1.4 s, giving the temporal memory of the catalytic communication.

The *significance* of these findings is that they demonstrate, *for the first time*, that long-range catalytic communication exists within single nanocatalysts; the communication distance can be up to a few hundred nanometers with a temporal memory of a few to tens of seconds. Although its mechanism remains to be elucidated, this catalytic communication is *phenomenologically* similar to cooperativity in enzymes, in which reactions occurring at one enzyme active site can affect reactions at other sites many angstroms to a few nanometers away within the same enzyme. Even though the catalytic communications observed here on Au@mSiO$_2$ nanocatalysts are weak, it would not be unreasonable to hypothesize that this catalytic communication may occur more effectively in other nanoscale catalysts — above all, there are a huge variety of them[25-27]. The generalization and further utilization of this effect can perhaps introduce a new paradigm in understanding, as well as developing, nanocatalysts.

VII. Progress in new direction: imaging catalytic reactivity at nanoscale metal–metal junctions

In the past year, we have also been studying the catalytic reactivity at nanoscale metal–metal junctions. Many nanoscale catalysts involve two, or more, metal components, and the interfaces, or the

junction areas, between two different metals are believed to have special catalytic activity that is not present for either of the metals alone. The synergistic effects and/or promoting effects at interfaces are often invoked to account for the observed catalytic enhancements of bimetallic nanoparticles (e.g., references[28-34]). Yet, *none of existing studies* quantify in a spatially resolved manner the catalytic reactivity at the interfacial region, and *little evidence* is available that clearly demonstrates reactions occur preferentially at the interfacial region relative to the non-interfacial regions in bimetallic nanocatalysts, let alone in further direct correlation with the interface structure and composition. Such lack of studies constitutes a significant knowledge gap, which not only impedes our fundamental understanding of the structure-reactivity correlations at metal-metal interfaces, but also limits our ability to develop effective bimetallic nanocatalysts with desired catalytic properties.

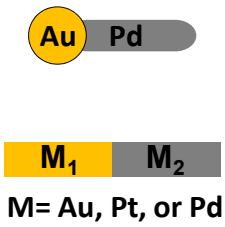

Fig 12. Schematic of a Au-nanoparticle-Pd-nanorod heteronuclear particle (top) and a bimetallic nanorod with two metal components (bottom). Both systems have a metal-metal junction.

Therefore, our *objective* here is to define the link between interface reactivity and interface structure/composition. The *rationale* for this research is that, once we understand quantitatively the reactivity-structure/composition correlation at metal-metal interfaces at the nanoscale, we will be able to design and engineer bimetallic nanoparticles with superior catalytic reactivity for desired chemical transformations.

We have chosen to work on *two model systems* (**Fig 12**): Au-nanoparticle-on-Pd-nanorod hetero-bimetallic nanoparticles and segmented M_1-M_2 multimetallic nanorods, where M_1 and M_2 are Au, Pt, Pd or alloy of them). We chose the first system as a model catalyst because of their controllable colloidal synthesis, tunable size, anisotropic structure with a defined Au-Pd interface, and highly crystalline in structure. We chose the second system as another model catalyst because of their versatile electrodeposition-based preparation in combining different metals to form defined interfaces, tunable size, tunable interface composition, and anisotropic structure. We are using the *approach* of single-molecule super-resolution fluorescence microscopy to quantify catalytic reactivity of single hetero-metallic nanocatalysts at nanometer spatial resolution and single-reaction temporal resolution, in combination with controlled and tunable sample synthesis as well as high-resolution interfacial structural/compositional characterizations.

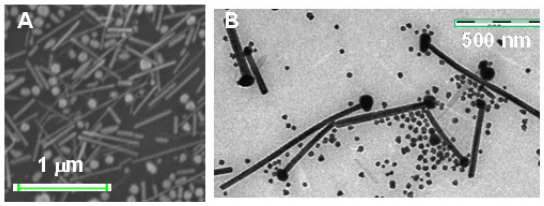

Fig 13. SEM images of Pd nanorods (A) and Au-Pd hetero-nanoparticles (B). The smaller particles in B are Pd particles.

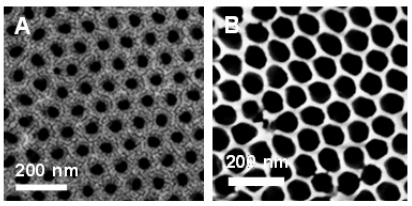

Fig 14. SEM images of the top surface of alumina membranes with pore sizes of ~40 nm (A) and ~80 nm (B) in diameter.

Regarding the 1st system, by following the procedure of Huang et al[35], we have made Pd nanorods of a few hundred nanometers in length and ~27 nm in diameter (**Fig 13A**). *The length is tunable with reaction time.* We have also successfully grown pseudo-spherical Au nanoparticles of ~100 nm in diameter at one end of the Pd nanorods (i.e., Au-Pd hetero-nanoparticles, **Fig 13B**), following the procedure in the same paper[35]. The size of the Au nanoparticle can be tuned by controlling growth time and reactant concentration. The samples are a mixture,

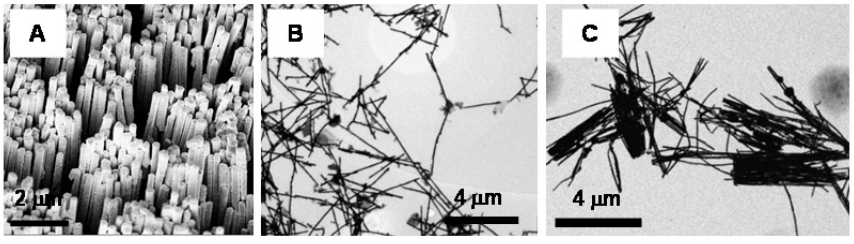

Fig 15. (A) SEM image of ~200 nm diameter Au nanorods. (B) TEM image of ~80 nm diameter Pt nanorods. (C) TEM image of ~80 nm diameter segmented bimetallic Au-Pt nanorods.

which, although not ideal for many applications, is *not* a problem for single-particle studies, as we can differentiate them in both electron microscopy and catalysis imaging. We have also tested these nanoparticles and they are active in catalyzing the reductive N-deoxygenation of resazurin.

Regarding the 2nd system, we have used templated electrodeposition[36-38] to make these segmented multimetallic nanorods. As the template, we found that the pore uniformity of the commercially available alumina membranes is only in good quality down to ~200 nm in diameter. In order to make segmented nanorods of smaller diameters, we followed the procedure by Masuda *et al.*[39] and successfully made alumina membranes with smaller and tunable pore sizes (e.g., ~40 nm and ~80 nm in diameter in **Fig 14**).

Using the alumina membranes and the templated electrodeposition approach, we have prepared monometallic Au and Pt nanorods of various diameters and a few μm in length (**Fig 15A, B**). The monometallic nanorods will be used as controls and comparisons for our study of segmented multimetallic nanorods. We have also made segmented Au-Pt bimetallic nanorods of ~80 nm in diameter, where the Au and Pt nanorod segments are approximately same in length (**Fig 15C**). We will perform detailed structural and compositional analysis on these segmented multimetallic nanorods.

Bibliography

1 X. Zhou, W. Xu, G. Liu, D. Panda & P. Chen. Size dependent catalytic activity and dynamics of gold nanoparticles at the single-molecule level. *J Am Chem Soc* **132**, 138-146 (2010).

2 X. Zhou, N. M. Andoy, G. Liu, E. Choudhary, K.-S. Han, H. Shen & P. Chen. Quantitative super-resolution imaging uncovers reactivity patterns on single nanocatalysts. *Nature Nanotech* **7**, 237–241 (2012).

3 N. M. Andoy, X. Zhou, E. Choudhary, H. Shen, G. Liu & P. Chen. Single-molecule catalysis mapping quantifies site-specific activity and uncovers radial activity gradient on single 2d nanocrystals. *J Am Chem Soc* **135**, 1845–1852 (2013).

4 X. Zhou, E. Choudhary, N. M. Andoy, N. Zou & P. Chen. Scalable parallel screening of catalyst activity at the single-particle level and sub-diffraction resolution. *ACS Catal* **3**, 1448-1453 (2013).

5 K. S. Han, G. Liu, X. Zhou, R. E. Medina & P. Chen. How does a single pt nanocatalyst behave in two different reactions? A single-molecule study. *Nano Lett* **12**, 1253-1259 (2012).

6 X. Zhou, N. M. Andoy, G. Liu & P. Chen. Long-range catalytic communication within single nanocatalysts. In revision.

7 W. Xu, H. Shen, G. Liu & P. Chen. Single-molecule kinetics of nanoparticle catalysis. *Nano Research* **2**, 911-922 (2009).

8 H. Shen, W. Xu & P. Chen. Single-molecule nanoscale electrocatalysis. *Phys Chem Chem Phys* **12**, 6555-6563 (2010).

9 P. Chen, X. Zhou, H. Shen, N. M. Andoy, E. Choudhary, K.-S. Han, G. Liu & W. Meng. Single-molecule fluorescence imaging of nanocatalystic processes. *Chem Soc Rev* **39**, 4560-4570 (2010).

10 P. Chen, X. Zhou, N. M. Andoy, K.-S. Han, E. Choudhary, N. Zou, G. Chen & H. Shen. Spatiotemporal catalytic dynamics within single nanocatalysts revealed by single-molecule microscopy. *Chem Soc Rev* **43**, 1107-1117 (2014).

11 E. Betzig, G. H. Patterson, R. Sougrat, O. W. Lindwasser, S. Olenych, J. S. Bonifacino, M. W. Davidson, J. Lippincott-Schwartz & H. F. Hess. Imaging intracellular fluorescent proteins at nanometer resolution. *Science* **313**, 1642-1645 (2006).

12 M. J. Rust, M. Bates & X. Zhuang. Sub-diffraction-limit imaging by stochastic optical reconstruction microscopy (storm). *Nature Meth* **3**, 793-796 (2006).

13 S. T. Hess, T. P. K. Girirajan & M. D. Mason. Ultra-high resolution imaging by fluorescence photoactivation localization microscopy. *Biophys J* **91**, 4258-4272 (2006).

14 A. Gulati, H. Liao & J. H. Hafner. Monitoring gold nanorod synthesis by localized surface plasmon resonance. *J Phys Chem B* **110**, 22323-22327 (2006).
15 G. A. Somorjai & Y. Li. *Introduction to surface chemistry and catalysis*. 2nd edn, (John Wiley & Sons, 2010).
16 B. Goris, S. Bals, W. V. d. Broek, E. Carbó-Argibay, S. Gómez-Graña, L. M. Liz-Marzán & G. V. Tendeloo. Atomic-scale determination of surface facets in gold nanorods. *Nature Mater* **11**, 930–935 (2012).
17 M. Grzelczak, J. Pérez-Juste, P. Mulvaney & L. M. Liz-Marzán. Shape control in gold nanoparticle synthesis. *Chem Soc Rev* **37**, 1783-1791 (2008).
18 J. E. Millstone, S. Park, K. L. Shuford, L. Qin, G. C. Schatz & C. A. Mirkin. Observation of a quadrupole plasmon mode for a colloidal solution of gold nanoprisms. *J Am Chem Soc* **127**, 5312-5313 (2005).
19 W. Xu, J. S. Kong, Y.-T. E. Yeh & P. Chen. Single-molecule nanocatalysis reveals heterogeneous reaction pathways and catalytic dynamics. *Nature Mater* **7**, 992-996 (2008).
20 W. Xu, J. S. Kong & P. Chen. Single-molecule kinetic theory of heterogeneous and enzyme catalysis. *J Phys Chem C* **113**, 2393-2404 (2009).
21 W. Xu, J. S. Kong & P. Chen. Probing the catalytic activity and heterogeneity of au-nanoparticles at the single-molecule level. *Phys Chem Chem Phys* **11**, 2767-2778 (2009).
22 R. A. van Santen. Complementary structure sensitive and insensitive catalytic relationship. *Acc Chem Res* **42**, 57-66 (2009).
23 J.-P. Changeux. Allostery and the monod-wyman-changeux model after 50 years. *Annu Rev Biochem* **41**, 103-133 (2012).
24 Q. Cui & M. Karplus. Allostery and cooperativity revisited. *Protein Sci* **17**, 1295-1307 (2008).
25 G. Ertl, H. Knözinger & J. Weitkamp. *Handbook of heterogeneous catalysis*. (VCH, 1997).
26 U. Heiz & U. Landman. *Nanocatalysis*. (Springer, 2007).
27 D. Astruc. *Nanoparticles and catalysis*. (Wiley-VCH, 2007).
28 H. Lee, S. E. Habas, G. A. Somorjai & P. Yang. Localized pd overgrowth on cubic pt nanocrystals for enhanced electrocatalytic oxidation of formic acid. *J Am Chem Soc* **130**, 5406-5407 (2008).
29 H. Zhang, T. Watanabe, M. Okumura, M. Haruta & N. Toshima. Catalytically highly active top gold atom on palladium nanocluster. *Nature Mater* **11**, 49–52 (2012).
30 B. E. Solsona, J. K. Edwards, P. Landon, A. F. Carley, A. Herzing, C. J. Kiely & G. J. Hutchings. Direct synthesis of hydrogen peroxide from h_2 and o_2 using al_2o_3 supported au-pd catalysts. *Chem Mater* **18**, 2689-2695 (2006).
31 R. Mu, Q. Fu, H. Xu, H. Zhang, Y. Huang, Z. Jiang, S. Zhang, D. Tan & X. Bao. Synergetic effect of surface and subsurface ni species at pt−ni bimetallic catalysts for co oxidation. *J Am Chem Soc* **133**, 1978–1986 (2011).
32 F. Liu, J. Y. Lee & W. Zhou. Template preparation of multisegment ptni nanorods as methanol electro-oxidation catalysts with adjustable bimetallic pair sites. *J Phys Chem B* **108**, 17959–17963 (2004).
33 C.-H. Cui, J.-W. Yu, H.-H. Li, M.-R. Gao, H.-W. Liang & S.-H. Yu. Remarkable enhancement of electrocatalytic activity by tuning the interface of pd-au bimetallic nanoparticle tubes. *ACS Nano* **5**, 4211–4218 (2011).
34 D. Mott, J. Luo, P. N. Njoki, Y. Lin, L. Wang & C.-J. Zhong. Synergistic activity of gold-platinum alloy nanoparticle catalysts. *Catal Today* **122**, 378-385 (2007).
35 X. Huang & N. Zheng. One-pot, high-yield synthesis of 5-fold twinned pd nanowires and nanorods. *J Am Chem Soc* **131**, 4602–4603 (2009).
36 C. R. Martin. Membrane-based synthesis of nanomaterials. *Chem Mater* **8**, 1739–1746 (1996).
37 D. Al-Mawlawi, C. Z. Liu & M. Moskovits. Nanowires formed in anodic oxide nanotemplates. *J Mater Res* **9**, 1014-1018 (1994).
38 B. R. Martin, D. J. Dermody, B. D. Reiss, M. Fang, L. A. Lyon, M. J. Natan & T. E. Mallouk. Orthogonal self-assembly on colloidal gold-platinum nanorods. *Adv Mater* **11**, 1021-1025 (1999).

39 H. Masuda & K. Fukuda. Ordered metal nanohole arrays made by a two-step replication of honeycomb structures of anodic alumina. *Science* **268**, 1466-1468 (1995).